

Primljen / Received: 20.3.2016.

Ispravljen / Corrected: 28.6.2016.

Prihvaćen / Accepted: 22.7.2016.

Dostupno online / Available online: 10.9.2016.

# Cyclic testing of single-span weak frames with masonry infill

## Authors:



**Goran Gazić**, PhD. CE.  
University of J.J. Strossmayer in Osijek  
Faculty of Civil Engineering Osijek  
ggazic@gfos.hr



Prof. **Vladimir Sigmund**

Original scientific paper

**Goran Gazić, Vladimir Sigmund**

## Cyclic testing of single-span weak frames with masonry infill

Experimental test results for fourteen samples of single-span, single-storey, non-seismically designed reinforced-concrete (weak) masonry infill frames are presented in the paper. The samples, scaled 1 to 2, were subjected to the approximately constant vertical and in-plane horizontal cyclic load. Various geometrical and mechanical properties of reinforced-concrete frames and masonry infill were considered. Equations for estimating the interstorey drift ratio at the limit states under study are proposed based on testing conducted in the paper.

### Ključne riječi:

weak reinforced-concrete frames, masonry infills, experimental research, behaviour of samples

Izvorni znanstveni rad

**Goran Gazić, Vladimir Sigmund**

## Ciklična ispitivanja jednorasponskih slabih okvira sa zidanom ispunom

U radu su prikazani rezultati eksperimentalnih istraživanja četrnaest uzoraka jednorasponskih, jednoetažnih, neseizmički projektiranih armiranobetonskih (slabih) okvira sa zidanom ispunom, izvedenih u mjerilu 1:2. Uzorci su ispitani pod približno konstantnim vertikalnim i ravninskim horizontalnim cikličnim opterećenjem. Promatrani su različiti parametri uzoraka u pogledu geometrijskih i mehaničkih karakteristika armiranobetonskih okvira i zidane ispune. Na temelju provedenih ispitivanja predložene su jednadžbe za procjenu relativnog međukatnog pomaka pri promatranim graničnim stanjima.

### Ključne riječi:

slabi armiranobetonski okviri, zidane ispune, eksperimentalna istraživanja, ponašanje uzoraka

Wissenschaftlicher Originalbeitrag

**Goran Gazić, Vladimir Sigmund**

## Zyklische Versuche an einfachen schwachen Rahmen mit Mauerwerksausfachung

In dieser Arbeit werden die Resultate experimenteller Versuche an 14 Proben im Massstab 1:2 ausgeführter, einfacher, einstöckiger, nicht für seismische Lasten ausgelegter (schwacher) Stahlbetonrahmen mit Mauerwerksausfachungen dargestellt. Die Proben wurden unter annähernd konstanten vertikalen und horizontalen zyklischen Lasten untersucht. Verschiedene Parameter in Bezug auf geometrische und mechanische Eigenschaften des Rahmens und der Mauerwerksausfachung wurden betrachtet. Aufgrund der durchgeführten Versuche wurden Gleichungen zur Abschätzung der relativen Stockwerksschiefstellung für die betrachteten Grenzzustände vorgeschlagen.

### Ključne riječi:

schwache Stahlbetonrahmen, Mauerwerksausfachung, experimentelle Versuche, Verhalten von Versuchsproben

### 1. Introduction

Reinforced concrete frames with masonry infill walls behave as a composite structural system ("framed-masonry") under lateral seismic load, and their behaviour is highly influenced by the interaction of their components. This behaviour was studied following recent strong earthquakes, (Northridge 1994; Kocaeli and Duzce 1999; Sumatra 2007; Wenchuan 2008; Christchurch 2011) [1-5]. Masonry infill walls exhibited both beneficial (an increase in stiffness, strength and energy dissipation capacity of the system) and detrimental (a decrease in drift capacity and an increase in base-shear) impacts, depending on characteristics of r/c frames and masonry infill walls in question.

A significant portion of the present-day building stock in earthquake prone areas round the world consists of moment resistant r/c frames infilled with unreinforced masonry walls, which are designed for gravity loads only ("weak frames"), [6-8]. Typical characteristics of these weak-framed structures are a small amount of longitudinal reinforcement in columns, inadequate amount of transverse reinforcement in potential hinge regions, non-ductile beam column joints, etc. [9-12]. These were rarely experimentally investigated [13-21] and there is a lack of code provisions [22] regarding their seismic assessment and strengthening interventions.

Fourteen different 1/2 scale specimens representing these structures were tested in the scope of an extensive experimental campaign. The models consisted of one-storey, one-bay weak-framed structures infilled with masonry walls. They were exposed to constant vertical and cyclic lateral load, and they included different parameters such as mechanical properties of the masonry infill, and various properties related to r/c frame elements.

The results revealed significant contribution of masonry infill to the weak frame behaviour in terms of stiffness, strength and energy dissipation capacity. The contribution of masonry infill was related to frame and masonry infill properties. The robustness of masonry units, defined as the ratio of net to gross cross sectional area of masonry unit, and mortar type, appeared to be the governing parameter for damage severity of masonry infill, as well as for overall structural behaviour. Detrimental effects of masonry infill on frame elements were observed only in the specimen with a transverse reinforcement ratio lower than that defined in Eurocode 2 [23].

### 2. Experimental investigation

#### 2.1. Introduction

The specimens (Table 1 and Figure 1) were grouped into four different series with the same r/c frame parameters. The same frame aspect ratio was kept, while the column to beam moment of inertia ratio, and reinforcement ratio of frame members were varied. The r/c frames were infilled with five different masonry wall types.

Weak frames were designed as moment resistant frames for gravity loads with properties similar to those generally encountered in common buildings. The scaling of the r/c frames was conducted according to similitude laws [24], and the frames were produced by a local construction company.

Table 1. Frame properties

Frame	$\alpha$	$\beta$	$\rho_{lc}$ [%]	$\rho_{tc}$ [%]	$\rho_{lb}$ [%]	$\rho_{tb}$ [%]
O1	0.75	0.42	1.0	0.13	3.8	0.13 (0.07)
O2	0.75	0.42	1.0	0.09	3.8	0.13 (0.07)
O3	0.75	1.95	1.0	0.13	3.8	0.13 (0.07)
O4	0.75	1.0	1.3	0.13	3.0	0.13 (0.07)

$\rho_{lc}$  and  $\rho_{tc}$  are the column's longitudinal and transverse reinforcement ratios  
 $\rho_{lb}$  and  $\rho_{tb}$  are the beam's longitudinal and transverse reinforcement ratios; transverse reinforcement ratios in the middle third of the beam length are given in parenthesis.

Two types of units were used for masonry walls: (1) solid clay units (*c* measuring  $b/h/l = 120/65/250$  mm) and (2) hollow clay masonry units (*b* – Group 2 according to Eurocode 6 [25], measuring  $b/h/l = 120/90/250$  mm). Three mortar types were used: (1) cement-lime mortar (*pm* with a volumetric ratio of cement:lime:sand = 1:1:5); (2) lime mortar (*vm* with a volumetric lime to sand ratio of 1:3); (3) no mortar. By combining these, five different masonry infill wall types were obtained (Table 2). Masonry infill walls were built with fully mortared bed and head joints of approximately 1 cm in depth/thickness. No additional connections, except connection by adhesion, were provided between the walls and the frame. Masonry units and mortar joints were not scaled according to similitude laws due to technical obstacles. The height of hollow units was kept to scale so as to keep the number of horizontal joints similar to that used in a prototype structure. Solid clay units were not scaled at all. According to [26], the damage mode or lateral strength is not influenced the up to 1/3 scaling of solid units.

Table 2. Masonry wall properties

Masonry wall	Label	Masonry unit	Mortar type
Strong	<i>cpm</i>	solid clay (c)	cement-lime (pm)
	<i>bpm</i>	hollow clay (b)	cement-lime (pm)
Weak	<i>bvm</i>	hollow clay (b)	lime (vm)
	<i>cvm</i>	solid clay (c)	lime (vm)
	<i>b</i>	hollow clay (b)	no mortar

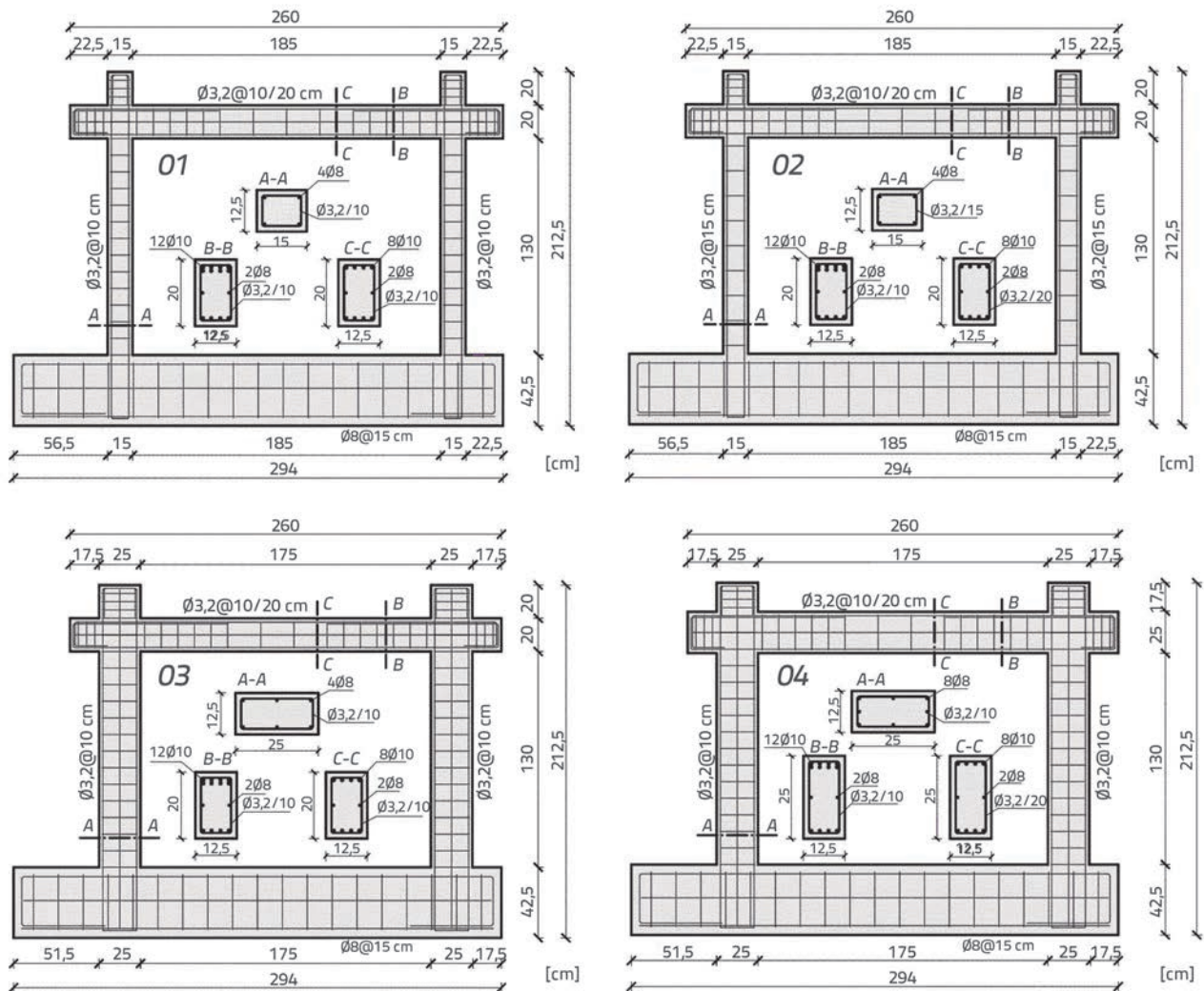


Figure 1. Frame specimens

Table 3. Tested specimens

Model	Type of frame	Type of masonry unit	Type of mortar
O1*	O1	-	-
O1_bpm	O1	hollow clay units	cement-lime
O1_bpm*	O1	hollow clay units	cement-lime
O1_cpm	O1	solid clay units	cement-lime
O1_bvm	O1	hollow clay units	lime
O1_cvm*	O1	solid clay units	lime
O1_b	O1	hollow units	-
O2_cpm	O2	solid clay units	cement-lime
O3	O3	-	-
O3_bpm	O3	hollow clay units	cement-lime
O3_cpm	O3	solid clay units	cement-lime
O4	O4	-	-
O4_bpm	O4	hollow clay units	cement-lime
O4_cpm	O4	solid clay units	cement-lime

\*Repaired model

By combining the r/c frame and masonry wall properties, 14 tested specimens were obtained (see Table 3). Additionally, specimen O1\_b had the r/c frame properties of group O1 infilled with hollow clay units and without mortar, while specimens O1\_bpm and O1\_bpm\* differed in terms of loading history (the difference was caused by load application error).

## 2.2. Test setup and instrumentation

Specimens were tested in a steel reaction frame fixed to a strong floor with lateral support. Their foundation beams were fixed to the reaction frame and sliding was prevented by steel restrainers. Tests were performed under an approximately constant vertical and in-plane cyclic lateral load up to failure. Vertical loads, corresponding to 30-40 % of the design compressive strength of concrete, were applied at each column end by hydraulic jacks placed on a sliding support, which enabled lateral displacement and prevented rotation. Cyclic lateral in-plane loading was applied at the beam end along its centroid axis by two hydraulic jacks (Figure 2).

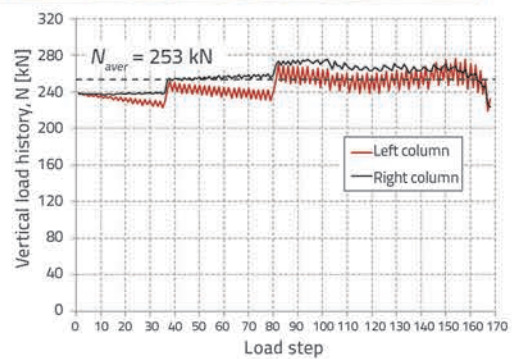
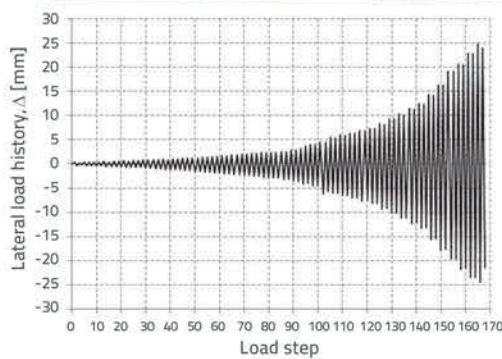
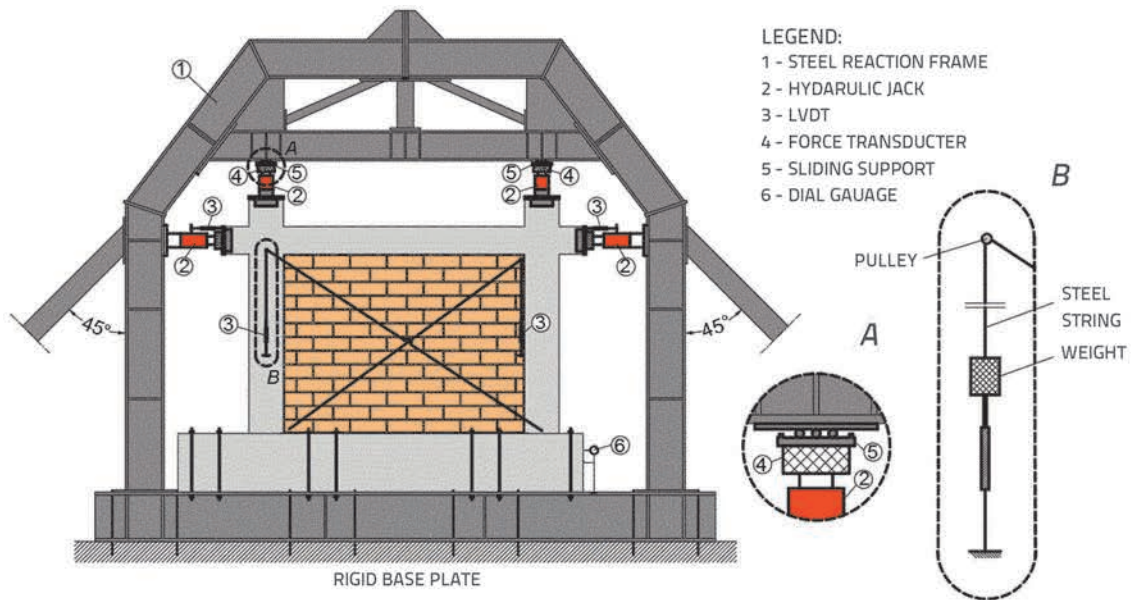


Figure 2. Test setup, instrumentation and loading history

Table 4. Constitutive material properties

Frame material properties				
Concrete C16/20	Longitudinal reinforcement S500		Transverse reinforcement S220	
Masonry infill properties				
	Masonry with cement-lime mortar		Masonry with lime mortar	
	Hollow clay units	Solid clay units	Hollow clay units	Solid clay units
$f_{mt}$ [MPa]	1.3	1.3	0.1	0.1
$f_m$ [MPa]	5.1	5.1	0.5	0.5
$f/f_b$ [MPa]	18.8/21.1	20.4/19.6	18.8/21.1	20.4/19.6
$f_j$ [MPa]	4.6	5.2	0.8	3.5
$f_t$ [MPa]	0.16	0.20	0.05	0.10
$E$ [MPa]	8188	1665	1766	1653
$f_{vo}$ [MPa]	0.42 (0.25)	0.18 (0.32)	0.13 (0.08)	0.04 (0.16)
$tg\alpha$	0.32	0.56	0.21	0.57

$f_{mt}$  and  $f_m$  are the tensile and compressive strength values for mortar.  $f$  and  $f_b$  are the compressive and normalized compressive strength values for masonry units  
 $f_j$ ,  $f_t$ ,  $E$  are the compressive strength, tensile strength, and modulus of elasticity values for masonry walls  
 $f_{vo}$ ,  $tg\alpha$  are the initial shear strength (cohesion) and angle of internal friction values for masonry walls. All values given in Table 4 are mean values.

The lateral load history consisted of the load (1) controlled in increments of 10 kN in a small deformation range, and displacement (2) controlled with gradually increasing displacements. Each loading cycle was repeated twice in order to capture the effects of stiffness and strength degradation. Loads were measured at each application point by force transducers, while horizontal displacements of the frame at both ends of the beam, and diagonal deformations of the frame and infill walls, were measured by LVDT's. A high-resolution dial gauge was used to monitor possible slippage of foundation beam. All measured data were continuously registered at a sampling rate of 0.01 sec by DEWE-30-16 system with DEWESoft ver. 6.6.7 software support. Deformations, cracks and their propagation were monitored visually and by the 3D optical measuring system ARAMIS.

### 3. Experimental results

#### 3.1. Material properties

All material properties, presented in Table 4, were tested according to current European standards. The concrete compressive strength was C16/20 according to [27], and the reinforcing steel properties were (S220) for transverse smooth bars and (S500) for longitudinal ribbed bars [28, 29]. All masonry wall properties were determined according to [30].

The shear strength of masonry was determined by shear test (Type A) on masonry triplets, and by diagonal test. The results given in parenthesis refer to shear strength determined by diagonal test. The results point to a significant influence of test method. The shear strength determined by shear test on masonry triplets (in literature referred to as cohesion) for

masonry walls made of hollow clay units was higher than the strength values determined by diagonal test, opposite to walls made of solid clay units. Deviations were expected since test methods are based on different hypotheses (different failure modes), but the differences were nevertheless surprising. An additional controversy was noticed. The tensile strength determined by diagonal test was higher than the shear strength determined by shear test on masonry triplets for masonry walls made of solid clay units. This was unexpected and related to different failure modes of tested masonry walls and texture of the masonry unit surface.

The reported masonry strengths show the predominance of robustness of masonry units and mortar type. Masonry walls made of cement-lime mortar exhibited higher values of tested properties compared to walls made of lime mortar. Similarly, masonry walls made of solid clay units exhibited higher values of tested properties, except modulus of elasticity, compared to the walls made of hollow clay units.

#### 3.2. Damage modes

Possible damage modes of the masonry infill wall and r/c frame are presented in Figures 3 and 4, according to [31, 32], and are correlated with three characteristic limit states of tested specimens.

The following limit states (LS) were defined for framed-masonry elements:

LS 1: Formation of first significant crack, defined by  $BS_{cr}$  and  $IDR_{cr}$ . The first significant crack was defined as the crack that propagates through at least four layers of masonry units (approximately one third of the infill height), or as the crack that crosses at least one half of the column depth.

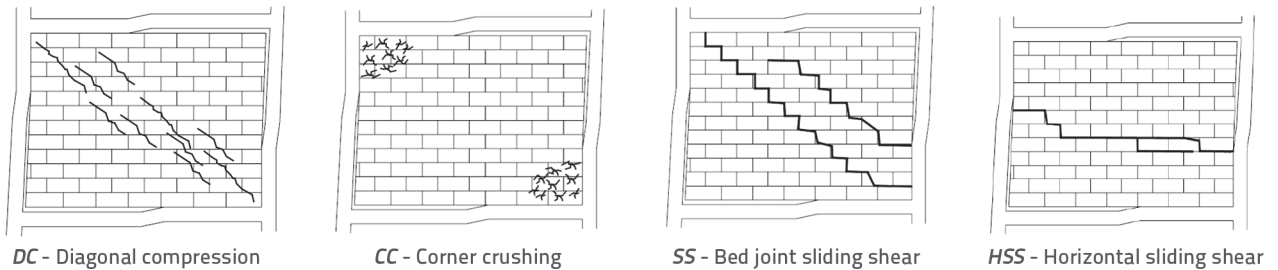


Figure 3. Damage modes of masonry infill, [32]

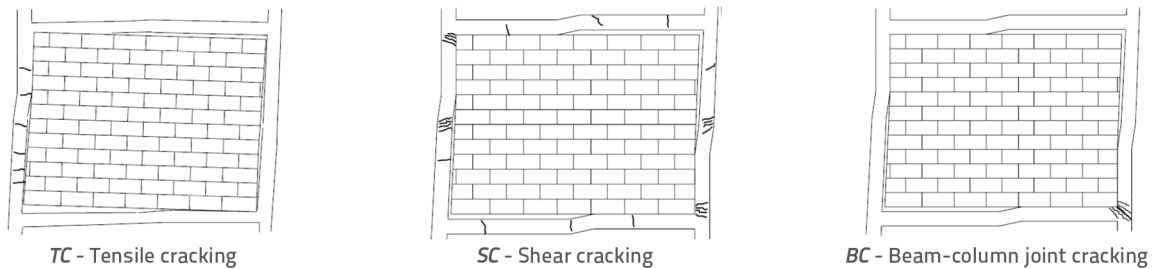


Figure 4. Damage modes of r/c frame, [32]

**LS<sub>2</sub>**: Initiation of yield, defined by  $BS_y$  and  $IDR_y$ , was determined by the appearance of the first crack that propagates through the entire infill, or by the load step in which cracks from opposite corners connect. For r/c frame, the initiation of yield was defined by the first crack that crosses the full column depth, or by the load step in which cracks from opposite column sides connect.

**LS<sub>3</sub>**: Composite action failure, defined by  $BS_f$  and  $IDR_f$ , was determined as failure of one of specimen components (frame or masonry infill), i.e. the load step that causes loss of composite action.

**BS** and **IDR** represent base-shear (lateral strength) and inter-storey drift at the corresponding **LS**, respectively. These limit states were noted as being the best ones for describing the observed response of specimens. Their primary curve is shown in Figure 5.

All tested specimens with hollow clay masonry units reached the maximum lateral strength at **LS<sub>2</sub>**, while those with solid clay masonry units reached this strength at **LS<sub>3</sub>**. The correlation between the limit states and damage modes is given in Table 5. Model *O1<sub>b</sub>* was omitted, since it had only **LS<sub>1</sub>**, regardless of a

relatively large drift of 1.7 %. Table 6 shows only representative drift values, the aim being to correlate different damage modes with limit states. The final crack patterns at maximum drifts are shown for all specimens in Figure 8.

Multiple failure modes of masonry infill occurred during the testing, which depended on the achieved drift (*IDR* %). The masonry infill properties, namely the mortar type and robustness of masonry units, appeared to be governing parameters for the severity of infill damage and overall behaviour.

Table 5. Correlation between limit states (LS) and damage modes

Model	LS <sub>1</sub>	LS <sub>2</sub>	LS <sub>3</sub>
<i>O1*</i>	TC	TC	SC
<i>O1<sub>bpm</sub></i>	DC	CC	CC (infill failure)
<i>O1<sub>bpm*</sub></i>	DC	CC	CC (infill failure)
<i>O1<sub>cpm</sub></i>	SS	HSS	SC (infill failure)
<i>O1<sub>bvm*</sub></i>	DC	HSS	CC (infill failure)
<i>O1<sub>cvm</sub></i>	SS	HSS	SC (frame failure)
<i>O2<sub>cpm</sub></i>	SS	HSS	SC (frame failure)
<i>O3</i>	TC	TC	SC
<i>O3<sub>bpm</sub></i>	DC	SS	CC (infill failure)
<i>O3<sub>cpm</sub></i>	SS	HSS	SC (frame failure)
<i>O4</i>	TC	TC	SC
<i>O4<sub>bpm</sub></i>	DC	SS	CC (infill failure)
<i>O4<sub>cpm</sub></i>	SS	HSS	SC (frame failure)

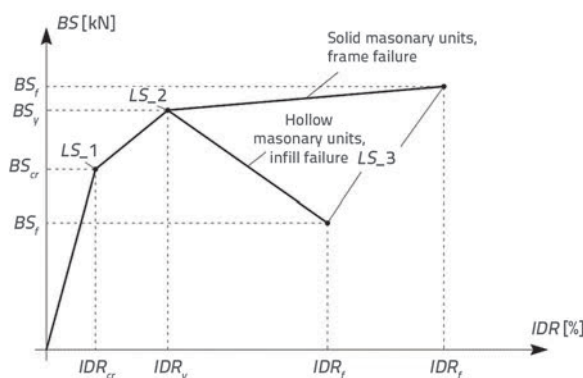


Figure 5. Primary curves and limit states of tested specimens

In specimens with hollow clay masonry units, a diagonal compression (*DC*) damage mode of the infill appeared at **LS<sub>1</sub>** as a diagonal crack located at upper corners and oriented at 65 - 70° from approximately one-half of the column's height. In *O1* specimens, the crushing of corners began at **LS<sub>2</sub>** and it

progressed until  $LS_3$  was reached. The central part of the infill wall remained undamaged. Although the out-of-plane tests were not performed, it can be concluded based on severity of damage (Figure 6.) that the out-of-plane stability of infill is highly questionable.

In the case of  $O3$  and  $O4$  specimens with hollow clay units,  $LS_1$  was the same as for  $O1$  specimens. At  $LS_2$ , diagonal cracks propagated throughout the infill from opposite corners through the mortar bed and head joints ( $SS$  damage mode). However, this change in damage mode did not cause significant difference in terms of global response. Regardless of the frame properties and type of masonry infill (strong or weak), the crushing of infill was a dominant damage mode at  $LS_3$ . The damage was concentrated at the frame-infill interface and along the shear failure plane, as shown in Figure 6. Furthermore, it caused significant degradation in lateral strength, composite action was lost, and the frame behaved independently at drifts in excess of 1%.

Similar behaviour was observed in the case of seismically designed r/c frames ("strong frames") infilled with masonry made of hollow clay units [33].

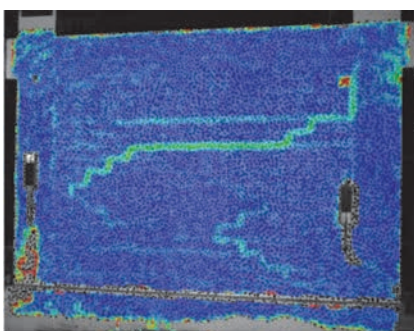
In the specimens with the infill made of solid clay units, the masonry infill walls maintained sufficient integrity during the

tests. Both limit states,  $LS_1$  and  $LS_2$ , were defined by the shear damage mode and only the transition from  $SS$  to  $HSS$  mode was observed, as shown in Figure 7. As the masonry infill did not crush, its participation in the lateral load resistance was maintained up to  $LS_3$ . The appearance of  $LS_3$  was determined by shear failure of r/c frame members. For specimens  $O1$  and  $O2$ , failure was caused by shear failure of one of the columns, while for specimens  $O3$  and  $O4$ , failure was caused by shear failure of beams.

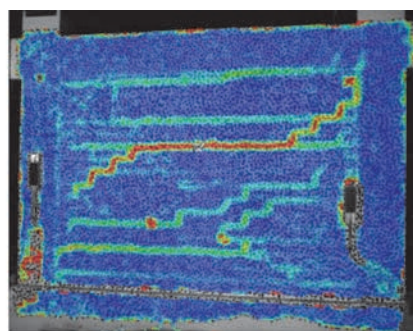
The ultimate failure of all r/c bare frames was caused by shear failure of one of the columns. The robust infill wall made with solid clay units contributed to the post-cracking load redistribution within the system and enhanced its strength and global stability. The damage mode prediction at  $LS_1$  could be established by comparing different damage modes of tested specimens reported in Table 5, and masonry strengths reported in Table 4. For masonry made of hollow clay units, the tensile strength determined by diagonal test had lower value than the shear strength determined by shear test on masonry triplets, regardless of mortar type, while the vice versa is true for masonry made of solid clay units. By calculating the ratio between these two strengths, it can be seen that the damage mode  $DC$  will occur for values higher than 1, while the damage mode  $SS$  will occur for



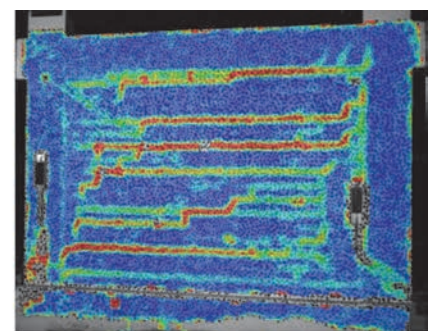
Figure 6. Failure of masonry infill walls made with hollow clay units (specimens  $O1_{bpm}$  and  $O3_{bpm}$ )



IDR = 0,15 %



IDR = 0,5 %



IDR = 1 %

Figure 7. Transition of damage modes in masonry infill wall made of solid clay units ( $O03_{cpm}$ , quantitative representation of relative deformation, ARAMIS)

values lower than 1. This observation needs to be further tested with shear to tensile strength ratios differing from those covered in presented study, especially for masonry made with hollow clay units ( $f_{vd}/f_t = 2,6$ ). Unfortunately, the same logic can not be applied for  $LS_2$ . The appearance of different damage modes at  $LS_2$  seems to be driven by mortar type and frame properties. The influence of mortar type can be seen by comparing damage modes of specimens  $O1_{bpm}$  and  $O1_{bvm}$ . Similarly, the influence of frame property, namely coefficient  $\beta$  (moment of inertia ratio), arises if damage modes of specimens  $O1_{bpm}$  and  $O3_{bpm}$  are compared. The influence of coefficient  $\beta$  could be explained with the "beam on elastic foundation" theory; an increase in coefficient  $\beta$  will cause an increase in the frame column stiffness relative to that of masonry infill, resulting in a different stress state within the masonry infill. A combined influence of mortar type and coefficient  $\beta$  on the initiation of damage mode at  $LS_2$  could not be determined.

Table 6 shows drift values at individual limit states (LS). These values were mainly influenced by masonry infill properties, i.e. mortar type and masonry unit robustness. In the case of strong masonry infill,  $LS_1$  occurred at the drifts of 0.15 %, regardless of unit type.  $LS_2$  occurred at the drifts of 0.30 % for hollow clay units, and at the drifts of 0.50 % for solid clay units.  $LS_3$  occurred at the drifts of 1 % and 1.5 % (from 1.35 to 1.70 %) for hollow and solid clay units, respectively.

For weak masonry infills, the mean drifts at  $LS_1$  were roughly a half of those observed for strong masonry infills, and they ranged from 0.06 to 0.085 %, with the mean value being 0.073. For the  $LS_2$  the drifts amounted to about 0.15 % for both unit types.  $LS_3$  drifts were about the same as those for strong masonry infills, and they depended on unit type.

**Table 6. Representative values of drift at individual limit states**

Limit states	Strong masonry infill		Weak masonry infill	
	Hollow clay units	Solid clay units	Hollow clay units	Solid clay units
$LS_1$ [%]	0.15	0.15	0.07	0.07
$LS_2$ [%]	0.3	0.5	0.15	0.15
$LS_3$ [%]	1.0	1.5	1.0	1.5

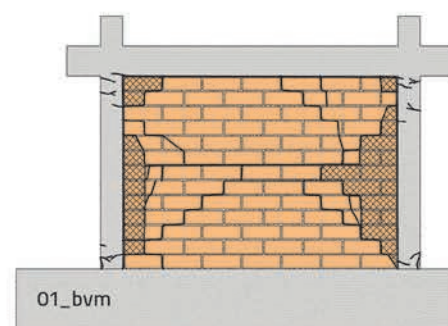
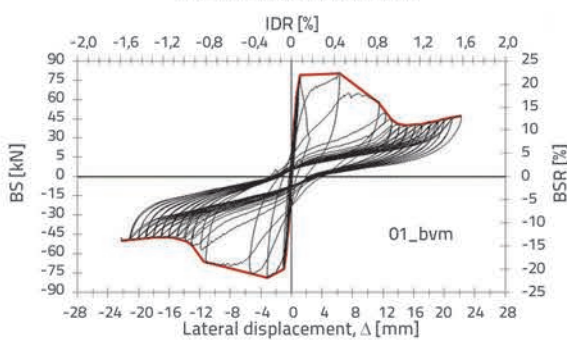
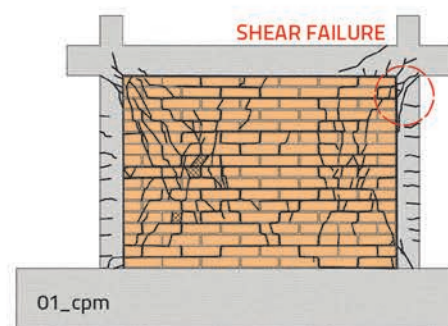
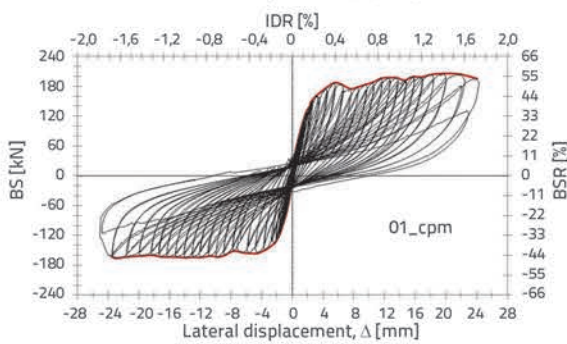
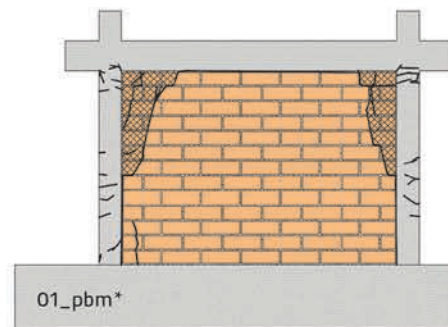
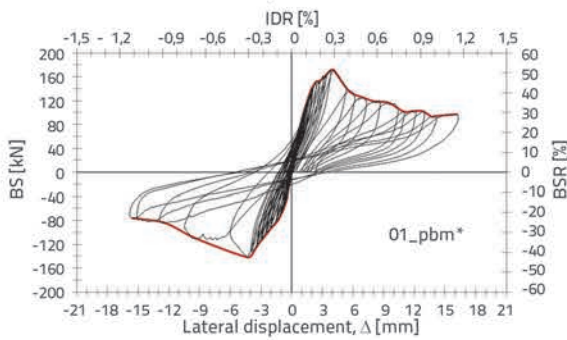
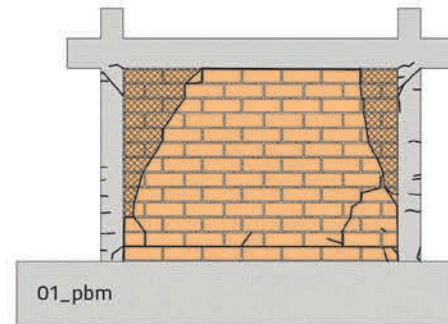
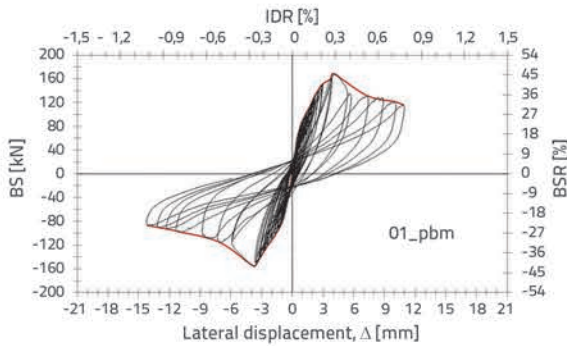
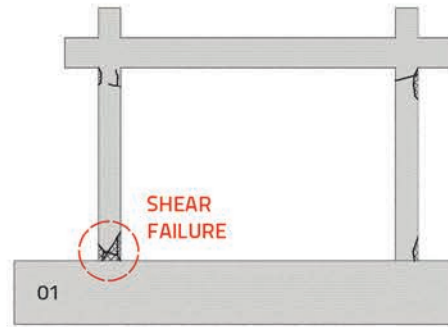
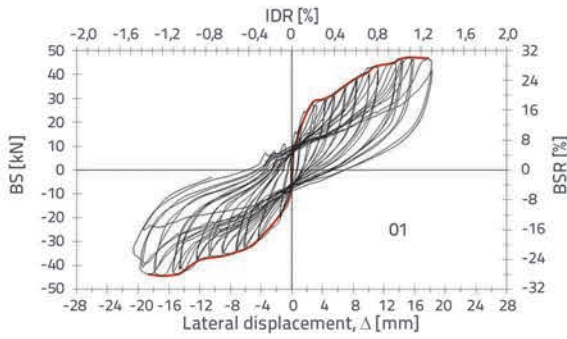
### 3.3. Hysteresis loops, response envelope curves and crack patterns

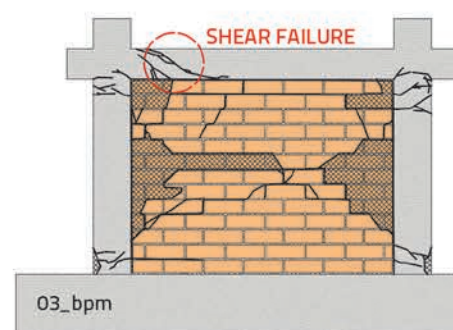
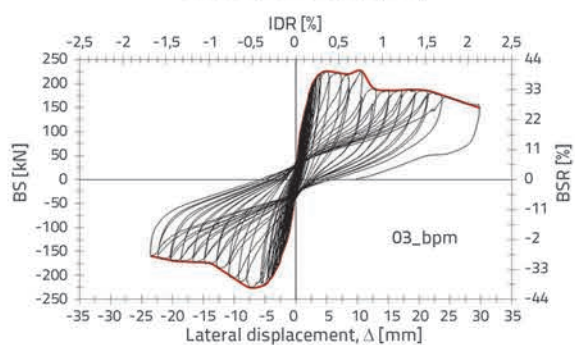
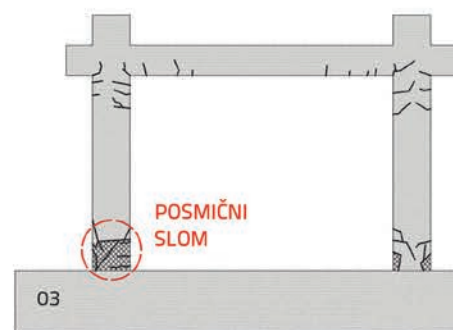
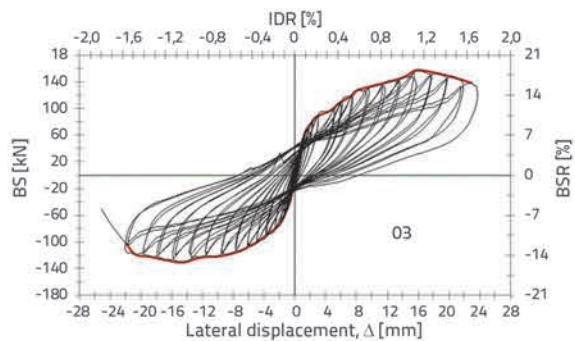
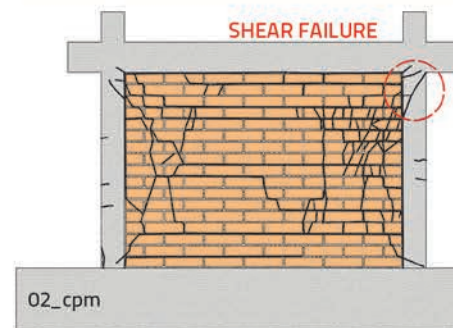
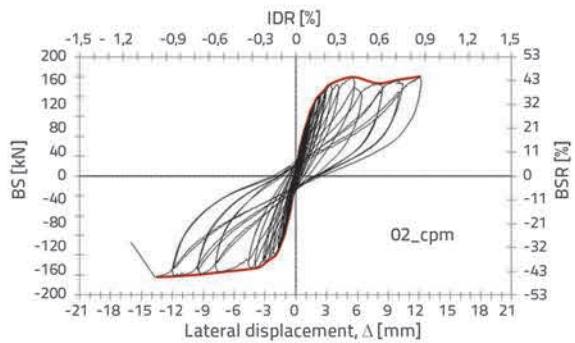
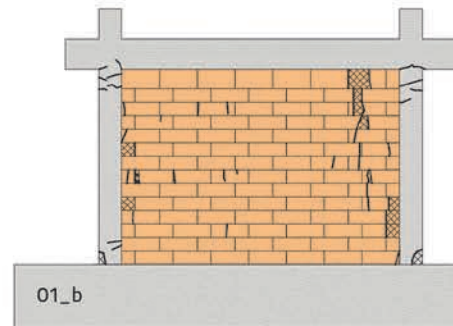
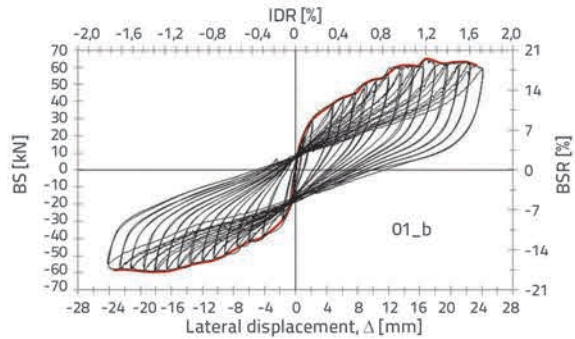
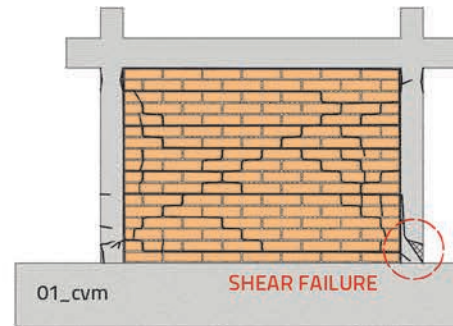
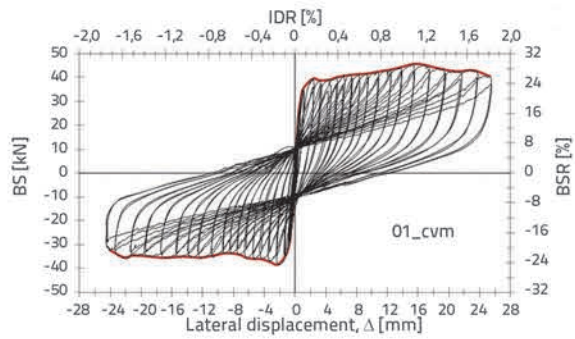
Measured hysteresis loops, response envelope curves, and crack patterns at maximum drifts are presented for all specimens in Figure 8. Lateral strengths, i.e.  $BS$  and the corresponding  $IDR$  for all specimens are presented at observed  $LS$  values in Table 7

**Table 7. Lateral strength i.e.  $BS$  [kN] and  $IDR$  [%] of specimens at corresponding  $LS$  values**

Model	Load direction +						Load direction -					
	$LS_1$		$LS_2$		$LS_3$		$LS_1$		$LS_2$		$LS_3$	
	$BS_{cr}$	$IDR_{cr}$	$BS_v$	$IDR_v$	$BS_f$	$IDR_f$	$BS_{cr}$	$IDR_{cr}$	$BS_v$	$IDR_v$	$BS_f$	$IDR_f$
*O1	28.1	0.19	43.3	0.81	46.7	1.31	29.1	0.31	37.5	0.88	-	-
$O1_{bpm}$	101.5	0.09	160.0	0.27	116.2	0.85	109.5	0.13	155.4	0.27	86.8	1.04
$O1_{bpm}^*$	105.6	0.08	170.6	0.27	94.2	1.00	97.0	0.15	141.5	0.31	83.8	0.88
$O1_{cpm}$	139.7	0.16	187.2	0.39	-	-	136.2	0.17	155.5	0.41	162.2	1.70
$O1_{bvm}$	71.0	0.06	78.7	0.08	39.7	1.00	66.2	0.06	78.8	0.16	48.5	1.06
* $O1_{cvm}$	70.8	0.08	79.1	0.16	81.2	1.80	69.4	0.09	76.6	0.18	-	-
$O2_{cpm}$	118.6	0.16	149.5	0.41	-	-	120.1	0.15	145.5	0.46	152.7	0.99
O3	94.8	0.23	142.5	0.96	-	-	105.3	0.43	130.5	1.07	103.0	1.62
$O3_{bpm}$	152.1	0.12	219.2	0.28	191.1	0.89	171.4	0.19	219.8	0.38	174.0	1.03
$O3_{cpm}$	148.9	0.15	279.9	0.50	-	-	180.0	0.19	280.2	0.56	298.9	1.35
O4	88.9	0.31	127.5	0.78	120.3	1.20	65.8	0.15	113.5	0.86	-	-
$O4_{bpm}$	200.9	0.16	258.5	0.28	184.7	0.93	219.6	0.20	258.8	0.29	172.0	0.94
$O4_{cpm}$	149.9	0.24	179.9	0.50	-	-	101.4	0.08	169.9	0.43	227.1	1.62







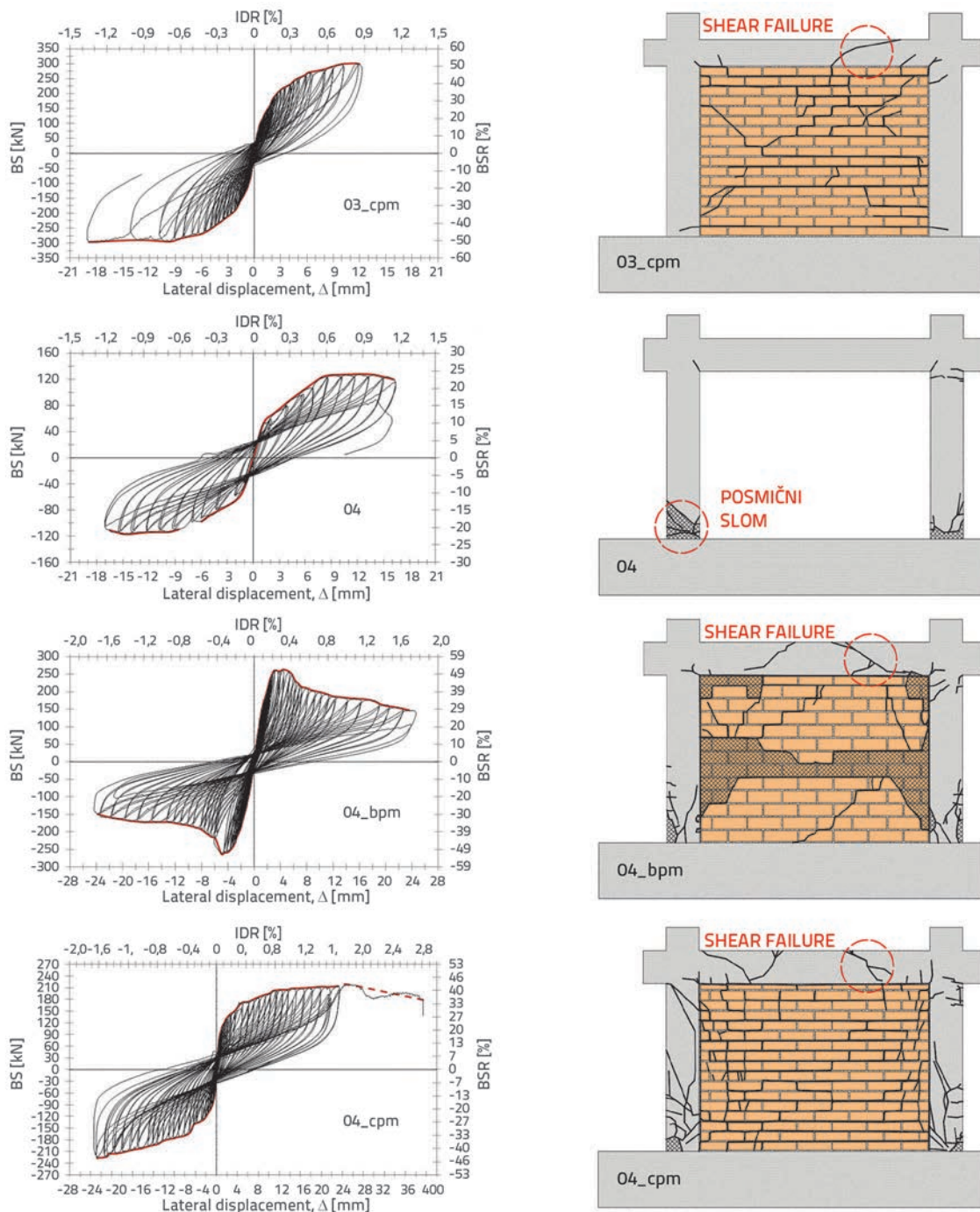


Figure 8 Hysteresis loops, response envelope curves and final crack patterns

for both loading directions. A positive direction is defined with positive values of  $BS$  and  $IDR$ . Model  $O1_b$  was not included, since only  $LS_1$  was observed.  $BSR$  represents the base shear ratio, and was defined as the lateral to vertical load ratio. The effective elastic stiffness,  $K_{EL}$ , was determined by  $LS_1$  for all specimens. The contribution of masonry infill to the effective elastic stiffness of a bare frame depended on the properties of such frame. The increase of the frame column moment of inertia, which is essentially an increase of the coefficient  $\beta$ , caused a

decrease in the masonry infill contribution. Consequently, the highest contribution was observed in the case of the weakest frame ( $O1$ ). Compared to effective elastic stiffness of the bare frame  $O1$ , the stiffness of specimens with infill made of hollow clay units increased by the factor of 8.8 (from 8.1 to 9.5). Surprisingly, the highest contribution was observed in case of infill made of lime mortar. This can be explained by a significantly smaller value of  $IDR$  at  $LS_1$ . The stiffness increased by a factor of 6.9 for specimens with solid clay units. In case

of specimens *O3*, the effective elastic stiffness increased by a factor of 3.3 and 2.9 for specimens with hollow and solid clay units, respectively. A similar trend was observed for specimens *O4*, with an increase by a factor of 3.3 and 2.6 for specimens with hollow and solid clay units, respectively. Contrary to bare frames, the variation of longitudinal reinforcement ratio in frame columns did not cause any significant differences in terms of stiffness of infilled specimens, since the response was dominated by masonry infill. According to Table 4, no masonry strength or modulus of elasticity could be directly related to stiffness contribution. However, a certain regularity can be observed if the masonry unit type is considered. The effective elastic stiffness is approximately equal for all specimens with hollow clay units as well as for those with solid clay units. For specimens with hollow clay units, the effective elastic stiffness ranged from 70 *kN/mm* to 85 *kN/mm*, while for specimens with solid clay units this value ranged from 59 *kN/mm* to 69 *kN/mm*. The higher values are related to specimens with stronger frames (*O3* and *O4*).

The contribution of masonry infill to the lateral strength of bare frames was influenced by both the frame and infill properties and depended on the achieved *IDR* value. The masonry infill contribution depended on mortar type, despite the fact that none of the masonry strengths reported in Table 4 could be directly related to strength contribution, and masonry unit robustness. The influence of mortar type on the lateral strength of specimens *O1* with hollow clay units is illustrated in Figure 9.

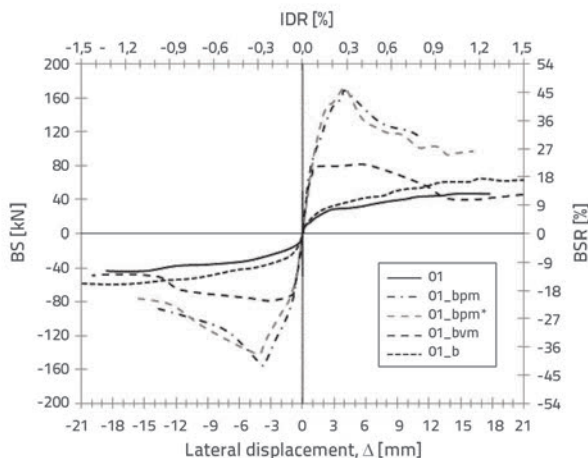


Figure 9. Influence of mortar type on lateral strength (BS) of specimens *O1*

The maximum *BS* of the specimen with cement-lime mortar was approximately 2 times greater than the maximum *BS* of the specimen with lime mortar. The difference between compressive strengths of masonry walls was approximately 5.7 times, while the difference between shear strengths (cohesion) amounted to approximately 3.2 times. The same difference in maximum *BS* was observed in the case of specimens with infill made of solid clay units (*O1\_cpm* and *O1\_cvm*), despite opposite trend in terms of the masonry wall compressive to shear and strengths ratio (1.5

and 4.5, respectively). An expected increase in lateral strength and stiffness was not observed despite the densely laid infill of model *O1\_b*, where a load transfer mechanism was provided by friction at the contact planes of units (as shown in Figure 10).

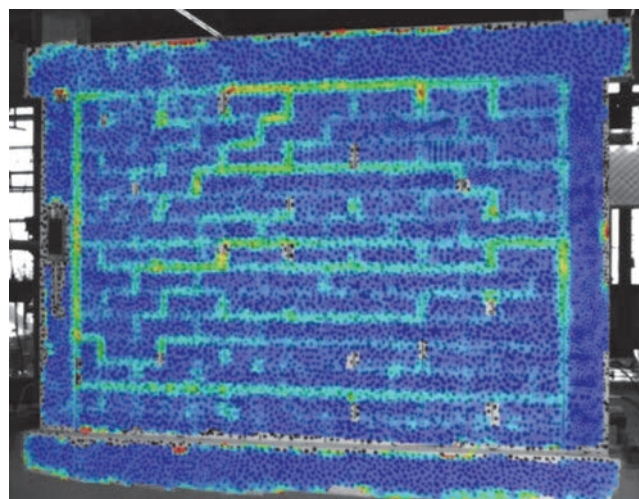


Figure 10. Strain distribution in masonry infill of specimen *O1\_b* (quantitative representation, relative deformation, ARAMIS)

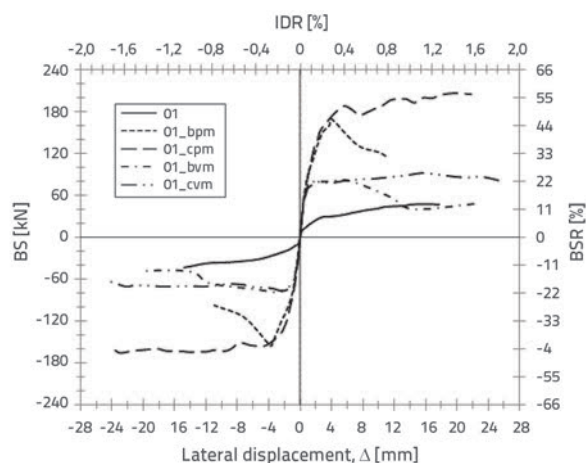


Figure 11. Influence of masonry unit robustness on lateral strength (BS) degradation of specimens *O1*

The maximum lateral strength increased by only 1.25 times and  $K_{EL}$  increased to 1.2 times the lateral strength and stiffness of the bare frame. Results indicated that the ductility increased by 1.3 times for the specimen *O1\_b* with regard to the bare frame. The model *O1\_b* was not subjected to load until failure.

The robustness of masonry units played a major role in terms of global response after *LS\_2* occurred. Regardless of mortar type and frame properties, all specimens with hollow clay units displayed strength degradation caused by infill crushing after *LS\_2* occurred, which ultimately led to bare frame behaviour. On the other hand, regardless of mortar type and frame properties,

all specimens with solid clay units maintained an approximately equal lateral strength after  $LS_2$  was reached. The influence of masonry unit robustness is illustrated by Figure 11 where lateral strengths of specimens  $O1$  with hollow and solid clay units are compared.

Since drift values at the  $LS$  of framed-masonry specimens and bare frames were significantly different, lateral strengths were normalized with regard to the lateral strength of the bare frame, as shown in Figure 12. This enabled evaluation of the masonry infill and frame properties contribution to the lateral strength (and stiffness) of framed-masonry specimens in the entire tested response range of bare frames.

The highest contribution of masonry infill was observed in the case of the weakest frame (frame  $O1$ ) and in the range of small drifts ( $IDR \leq 0.5\%$ ), where strong masonry infill increased the specimen's lateral strength by roughly 5.5 times. The contribution of the weak masonry infill in the range of small drifts ( $IDR \leq 0.15\%$ ) amounted to about 3.8 times. Regardless of the type of masonry infill (strong or weak), the strength and stiffness degradation was pronounced after the  $LS_2$  was reached, especially in the case of masonry infill made with hollow clay units. This behaviour implies significant influence of the masonry unit robustness on the degradation of strength and on global behaviour of the specimens.

In the case of frames  $O3$ , the masonry infill contribution in the small drift range ( $IDR \leq 0.5\%$ ) was about 2.2 times, while it was about 3 times for the frame  $O4$ . The contribution of masonry infill made with solid clay units was lower in the small drift range for specimens  $O4$ , which was caused by an unknown mechanism. An increase in the frame coefficient  $\beta$  (frame column height) caused a decrease in the masonry infill strength contribution (compare specimens  $O1$  and  $O3$ ), while an increase in the frame column longitudinal reinforcement ratio (compare specimens  $O3$  and  $O4$ ) did not cause major differences since the response was dominated by masonry infill.

The same trend of global behaviour regarding the masonry unit robustness was observed for all tested specimens. For all types of masonry infill, except in the case of  $O2_{cpm}$ , the ductility of framed-masonry specimens was approximately equal to or slightly higher than that of bare frames, as shown in Figures 11 and 13.

A special attention was given to model  $O2_{cpm}$ , as the detrimental influence of masonry infill in case of inadequate transverse reinforcement appeared to be of paramount importance. Its response was compared to model  $O1_{cpm}$ , which was designed with minimum transverse reinforcement according to [30]. A comparison of their response envelope curves is given in Figure 14. Both specimens had similar lateral strength and drifts at  $LS_1$  and  $LS_2$ . However, the

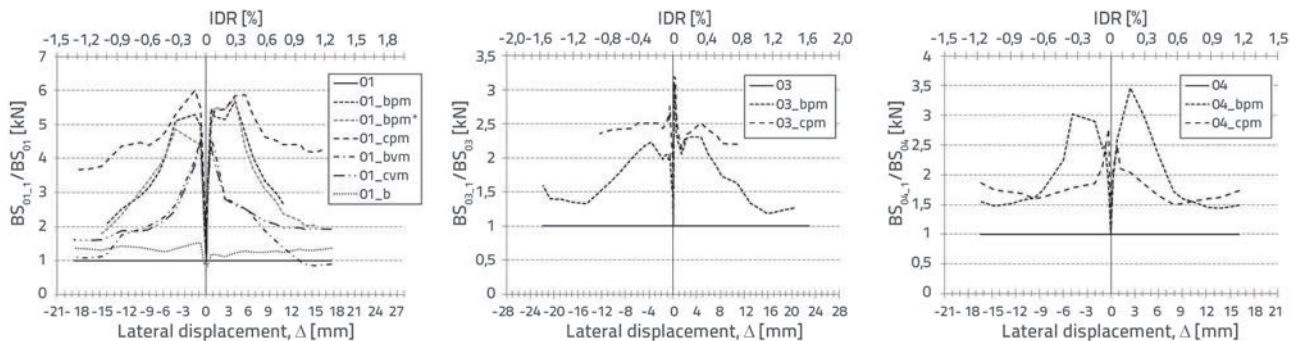


Figure 12. Lateral strength ( $BS$ ) of framed-masonry specimens normalized with regard to lateral strength of bare frames

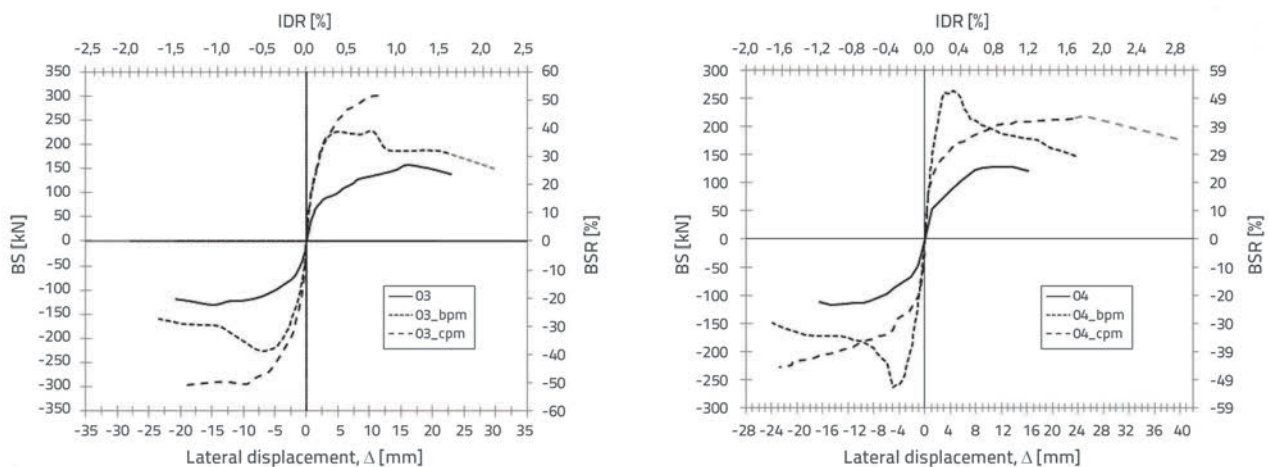


Figure 13. Response envelope curves of tested specimens

drift at  $LS_3$  for model  $O2\_cpm$  was significantly smaller. A 50 % reduction in transverse reinforcement ratio in columns caused a 70 % reduction in ultimate drift. The noted difference in the drifts of models  $O1\_cpm$  and  $O2\_cpm$  and the ductility of framed-masonry models (Figure 13) implied that the minimum transverse reinforcement ratio, as prescribed in the non-seismic code [23], could be sufficient for preventing a premature shear failure of columns in existing buildings, as caused by detrimental influence of masonry infill. This requires additional research that would need to focus on different transverse reinforcement ratios, concrete compressive strength and masonry infill properties, with an emphasis on masonry unit robustness. The observed behaviour of specimen  $O2\_cpm$  revealed yet another feature. Following the shear/axial failure of one of the columns, the specimen maintained a significant portion of the pre-failure lateral strength by losing only 75 % of its lateral strength, as shown in Figure 15. This can be attributed to the redistribution of vertical load within the framed-masonry elements. The infill had taken a higher vertical load and this increased shear friction within the infill, thus increasing its shear load carrying capacity. The masonry infill maintained sufficient integrity during the test, despite suffering heavy damage. No out-of-plane instabilities were observed. The infill contributed to the overall post-failure load carrying capacity and stability of the specimen.

### 3.4. Energy dissipation capacity

Specimen energy dissipation capacities are shown in Figure 16. In order to obtain the energy dissipated per unit drift, the hysteretic energy dissipated at each loading cycle was computed based on the area bounded by the hysteretic loop and divided by twice the peak drift. These values were then normalized to the energy dissipation capacity of bare frames.

The energy dissipation capacity was influenced by the infill and frame properties and depended on the achieved  $IDR$ . The maximum values corresponded approximately to drifts at  $LS_2$ . The masonry infill contribution was influenced by mortar type and masonry unit robustness. The influence of mortar type is illustrated by figure representing the energy dissipation capacity of specimens  $O1$ . Specimens with cement-lime mortar had a greater energy dissipation capacity than those made with lime mortar. After the  $LS_2$  was reached, the dissipation capacity was governed by masonry unit robustness. For all specimens with hollow clay units, a gradual decrease of the energy dissipation capacity was observed up to drifts of approximately 1 %. After that, the energy dissipation capacity was approximately equal to that of bare frame. On the other hand, the infill made of robust solid clay units maintained a ductile inelastic response and provided a more stable energy dissipation after the  $LS_2$  was reached.

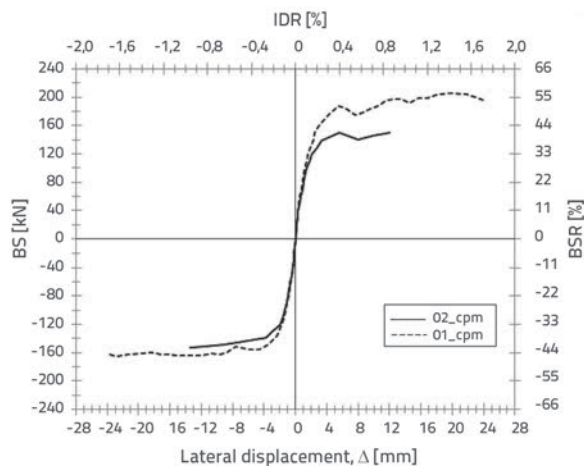


Figure 14. Response envelope curves of specimens

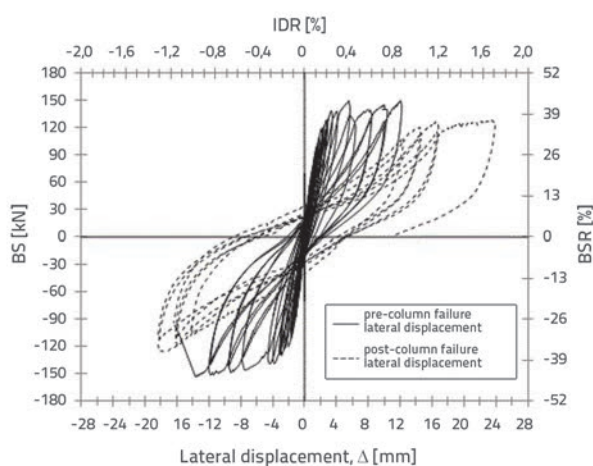


Figure 15. Hysteresis loops of specimen  $O2\_cpm$

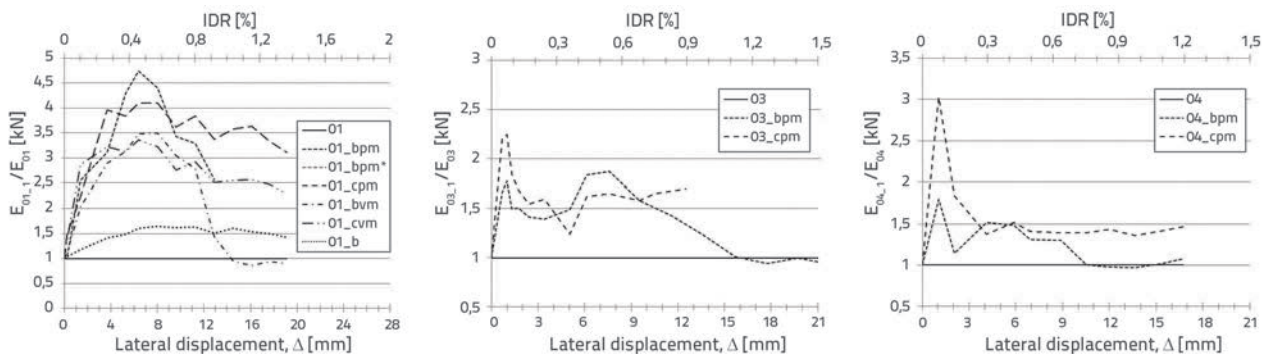


Figure 16. Energy dissipation capacity expressed per unit drift

An increase in the moment of inertia ratio  $\beta$  caused a decrease in masonry infill contribution. The variation of the longitudinal reinforcement ratio of the frame columns (specimens *O3* and *O4*) did not cause significant differences.

#### 4. Prediction of expected drift

Based on the observations made in Section 3, an attempt was made to define equations for the prediction of the  $IDR_s$  at limit states  $LS_1$  and  $LS_2$ . Since masonry strengths were influenced by mortar type and masonry unit robustness, they have caused a similar percentage of change in the  $IDR$  values. However, compared to other strengths, cohesion gave the smallest correlation coefficient when linear regression was made ( $R^2 = 0.8$  for  $LS_1$  and  $0.85$  for  $LS_2$ ). The influence of coefficient  $\beta$  was examined in the same manner. Although correlation coefficients were not satisfactory, the coefficient  $\beta$  was considered due to its obvious influence. Two equations were proposed: (1) for drifts at  $LS_1$  ( $IDR_{cr}$ ); (2) for drifts at  $LS_2$  ( $IDR_y$ ). A comparison of the experimentally obtained values and their analytical predictions are shown in Figures 17 (a) and (b). Suggested equations match the observed drifts with a satisfactory accuracy, and they generally tend to overestimate drifts for specimens with hollow clay units and underestimate drifts for specimens with solid clay units. The highest error in case of the  $LS_1$  amounted to  $-20.7\%$  and was observed for specimen *O1\_bvm*. In case of the  $LS_2$  the highest error was observed for specimen *O3\_cpm*, and it amounted to  $22.6\%$ . All other errors, for both  $LS_s$ , were lower than  $\pm 16\%$ .

The proposed equations do not have any physical meaning, and they were derived based on the performed experiments. They had to be tested for different values of  $f_{vo}$  (cohesion) and  $\beta$ . In addition, the influence of aspect ratio needs to be tested despite contradictions reported in literature, [18, 20]. Nevertheless, due to relative simplicity of proposed equations, they could be used for common masonry units and mortar types, as was the case in this study.

$$IDR_{cr} = 0,03 \cdot \beta + 0,7 \cdot f_{vo} \text{ [MPa]} \quad (1)$$

$$IDR_y = 0,05 \cdot \beta + 1,8 \cdot f_{vo} \text{ [MPa]} \quad (2)$$

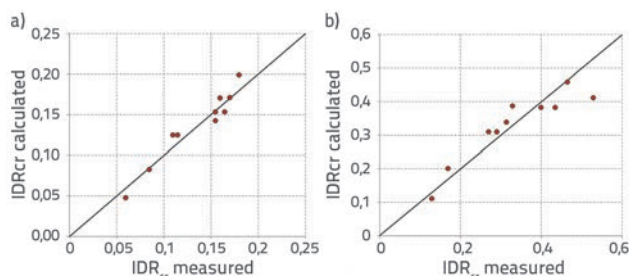


Figure 17. Comparison of experimental results and analytical predictions

#### 5. Conclusions

Fourteen 1/2 scaled one-span, one-storey specimens of the non-seismically designed weak r/c frames infilled with masonry walls (framed-masonry) were tested under constant vertical and in-plane cyclic lateral load. The specimens were divided into four series according to their frame properties, and were infilled with masonry infill walls of different properties. Their properties were those generally encountered in real buildings and the obtained results are applicable for assessing behaviour and strengthening of existing framed-masonry buildings.

Damage modes of framed-masonry specimens were defined. The robustness of masonry units and mortar type appeared to be the governing parameters for determining severity of damage to masonry infill and an overall behaviour of tested specimens. Severe crushing of masonry infill made of hollow clay units caused their out-of-plane instability and ultimately led to bare frame behaviour at 1% drifts. The masonry infill made of solid clay units maintained integrity throughout the testing (up to 1.5% drifts) and exhibited stable nonlinear response and energy dissipation.

Detrimental effects of masonry infill on frame elements were observed only in the case of a specimen with a transverse reinforcement ratio lower than the minimum prescribed by the non-seismic Eurocode 2. Here, a 50% reduction of transverse reinforcement ratio in the columns caused a 70% reduction in maximum drift, implying that the minimum transverse reinforcement ratio could be sufficient for preventing premature shear failure of columns, due to the presence of the infill (further testing is however needed).

The contribution of masonry infill was generally related to the frame and masonry infill properties. The effective elastic stiffness of bare frames increased from 3.8 to 9.5 times in the case of infill with hollow clay units, and from 3.4 to 5.8 times in case of infill with solid clay units, depending on frame properties. No significant differences were observed with regard to masonry strengths determined by testing. The contribution of masonry infill to the system strength was related to mortar type, but was not proportional to the strengths registered for masonry infill. Strong masonry infill increased the lateral strength of bare frames from 2.2 to 5.5 at 0.5% drifts, depending on frame properties. Weak masonry infill increased the system lateral strength roughly 3.8 times at 0.15% drifts.

The energy dissipation capacity of specimens was related to the masonry infill and frame properties. The contribution of brittle masonry infill made of hollow clay units was lost at 1% drifts. On the other hand, masonry infill made of solid clay units provided stable energy dissipation within the tested drift range (up to 1.5%).

The equations for predicting expected drifts at cracking and yielding points were derived using basic characteristics of the masonry infill and r/c frame. These provided a good match for the measured values and can be used as a convenient tool for reasonable prediction/estimation of the expected drifts of framed-masonry structures.

## Acknowledgements

The research presented in this paper is a part of the research project No. IP-11-2013-3013, entitled "Frame-masonry for modelling and standardization", funded by the Croatian Science Foundation, the support of which is gratefully acknowledged.

## REFERENCES

- [1] EERI: 1994 Northridge Earthquake Reconnaissance Report. *Earthquake Spectra* 12, (S1, S2), 1996.
- [2] EERI, 1999 Kocaeli, Turkey Earthquake Reconnaissance Report, *Earthquake Spectra* 16, (S1), 2000.
- [3] Maidiawati, Sanada, Y.: Investigation and Analysis of Buildings Damaged during the September 2007 Sumatra, Indonesia Earthquakes. *Journal of Asian Architecture and Building Engineering*, 7 (2008) 2, pp. 371-378.
- [4] Li, B., Wang, Z., Mosalam, K.M., Xie, H.: Wenchuan Earthquake Field Reconnaissance on Reinforced Concrete Framed Buildings With and Without Masonry Infill Walls. 14WCEE, *The 14<sup>th</sup> World Conference on Earthquake Engineering*, 2008.
- [5] Kam, W. Y., Pampanin, S., Elwood, K.: Seismic Performance of Reinforced Concrete Buildings in the 22 February Christchurch (Lyttelton) Earthquake, *Bulletin of the New Zealand Society for Earthquake Engineering*, 44 (2011) 4, pp. 239-278.
- [6] Bell, D. K., Davidson, B. J.: Evaluation of Earthquake Risk Buildings with Masonry Infill Panels, *NZSEE 2001. Conference*, Paper No.4.02.01. 2001.
- [7] Anagnos, T., Comerio, M.C., Goulet, C., Steele, J., Stewart J.P.: Development of a Concrete Building Inventory: Los Angeles Case Study for the Analysis of Collapse Risk, *Proceedings of 9th National & 10th Canadian Conference on Earthquake Engineering*, 2010.
- [8] Vintzileou, E., Zeris, C., Repapis, C.: Seismic Behaviour of Existing RC Buildings, *13th World Conference on Earthquake Engineering*, Paper No.2453, 2004.
- [9] Liel, A.B., Haselton, C.B., Deierlein, G.G.: Seismic Collapse Safety of Reinforced Concrete Buildings. 2: Comparative Assessment of Nonductile and Ductile Moment Frames, *Journal of Structural Engineering*, 135 (2011) 4, pp. 492-502.
- [10] Masi, A.: Seismic Vulnerability Assessment of Gravity Load Designed R/C Frames. *Bulletin of Earthquake Engineering*, 1 (2003), pp. 371-395, <http://dx.doi.org/10.1023/B:BEEE.0000021426.31223.60>
- [11] Hoffmann, G.W., Kunnath, S.K., Reinhorn, A.M., Mander, J.B.: Gravity-Load-Designed Reinforced Buildings: Seismic Evaluation of Existing Construction and Detailing Strategies for Improved Seismic Resistance. *Technical Report NCEER-92-0016*, 1992.
- [12] Jeon, J.S., Lowes, L.N., DesRoches, R., Brilakis I.: Fragility curves for non-ductile reinforced concrete frames that exhibit different response mechanisms, *Engineering Structures*, 15 (2015), pp. 127-143, <http://dx.doi.org/10.1016/j.engstruct.2014.12.009>
- [13] Fiorato, A.E., Sozen, M.A., Gamble, W.L.: An Investigation of the Interaction of Reinforced Concrete Frames with Masonry Filler Walls. *Technical Report UILU-ENG 70-100*, University of Illinois at Urbana-Champaign, 1970.
- [14] Mehrabi, A.B., Shing, P.B., Schuller, M. P., Nolan, J. L.: Performance of masonry-infilled R/C frames under in-plane lateral loads. *Report No. CU/SR-94/6*, University of Colorado at Boulder, 1994.
- [15] Buonopane, S.G., White, R.N.: Pseudodynamic Testing of Masonry Infilled Reinforced Concrete Frame. *Journal of Structural Engineering*, 125 (1999) 6, pp. 578-589.
- [16] Al-Chaar, G., Issa, M., Sweeney, S.: Behavior of Masonry-Infilled Nonductile Reinforced Concrete Frames. *Journal of Structural Engineering*, 128 (2002) 8, 1055-1063, 2002.
- [17] Colangelo, F.: Experimental Evaluation of Member-by-Member Models and Damage Indices for Infilled Frames. *Journal of Earthquake Engineering*, 7 (1), pp. 25-50, <http://dx.doi.org/10.1080/13632460309350440>
- [18] Colangelo, F.: Pseudo-dynamic seismic response of reinforced concrete frames infilled with non-structural brick masonry. *Earthquake Engineering and Structural Dynamics*, 34 (2005), pp. 1219-1241, <http://dx.doi.org/10.1002/eqe.477>
- [19] Centeno, J., Ventura, C. E., Foo, S.: In-plane Shake Table Testing of Gravity Load Designed Reinforced Concrete Frames with Unreinforced Masonry Infill Walls. *Proceedings of 14th World Conference on Earthquake Engineering*, 2008.
- [20] Stavridis, A.: Analytical and Experimental Study on Seismic Performance of Reinforced Concrete Frames Infilled with Masonry Walls. *Doctoral Dissertation*, University of California at San Diego, 2009.
- [21] Pujol, S., Fick, D.: The test of a full-scale three-storey RC structure with masonry infill walls. *Engineering Structures*, 32 (2010) 10, pp. 3112-3121.
- [22] CEN, Eurocode 8 – Design of Structures for Earthquake Resistance. Part 3: Assessment and Retrofitting of Buildings, Brussels, 2004.
- [23] CEN, Eurocode 2 – Design of Concrete Structures. Part 1-1: General Rules and Rules for Buildings, Brussels, 2004.
- [24] Harris, H.G., Sabnis G. M.: Structural Modeling and Experimental Techniques. *CRC Press*, Boca Raton, FL. 1999., <http://dx.doi.org/10.1201/9781420049589>
- [25] CEN, Eurocode 6 – Design of Masonry Structures. Part 1-1: General Rules for Reinforced and Unreinforced Masonry, Brussels, 2005.
- [26] Dakudze, A.: Behaviour of Reinforced Concrete Frames Infilled with Brick Masonry Panels. *Doctoral Dissertation*, The University of New Brunswick, 2000.
- [27] CEN, EN 12504 – Testing Concrete in Structures. Part 1: Cored Specimens – Taking, Examining and Testing in Compression, Brussels, 2000.



- [28] International standard ISO 6892 – 1: Metallic Materials – Tensile Testing. Part 1: Method of Test at Room Temperature, Geneva, 2009.
- [29] Tomičić, I.: Betonske konstrukcije, DHGK, Zagreb, 1996.
- [30] Penava, D., Radić, I., Gazić, G., Sigmund, V.: Mechanical Properties of Masonry as Required for the Seismic Resistance Verification. *Technical Gazette*, 18 (2011) 2, pp. 273-280.
- [31] Haldar, P., Singh, Y., Paul, D. K.: Identification of Seismic Failure Modes of URM Infilled RC Frame Buildings. *Engineering Failure Analysis*, 33 (2013), pp. 97-118, <http://dx.doi.org/10.1016/j.engfailanal.2013.04.017>
- [32] Kalman-Šipoš, T., Sigmund, V., Hadzima-Nyarko, M.: Earthquake Performance of Infilled Frames Using Neural Networks and Experimental Database. *Engineering Structures*, 51 (2013), pp. 113-127.
- [33] Zovkic, J., Sigmund, V., Guljaš, I.: Cyclic Testing of a Single Bay Reinforced Concrete Frames With Various Types of Masonry Infill. *Earthquake Engineering and Structural Dynamics*, 42 (2013) 8, pp. 1131-1149.